

Green and Facile Synthesis of Porous Hierarchical Cr₂O₃/N-doped Carbon Composite with High Li-Ion Battery Anodic Performance

Shuang Ma¹, Yingming Xu¹, Xiaoli Cheng¹, Xianfa Zhang^{1,*}, Shan Gao¹, Hui Zhao¹, Lihua Huo^{1,*}

Key Laboratory of Functional Inorganic Material Chemistry, Ministry of Education, School of Chemistry and Materials Science, Heilongjiang University, Harbin 150080, PR China

*E-mail: lhhuo68@163.com, zhangxf_1982@126.com

Received: 2 February 2018 / Accepted: 15 March 2018 / Published: 10 May 2018

A green and facile bio-template method was developed to synthesize porous hierarchical Cr₂O₃/N-doped carbon (denoted as Cr₂O₃/NC) composite using egg-shell membrane as template and carbon source. The as-prepared Cr₂O₃/NC composite is assembled from interwoven and coalesced porous microfibers. The microfibers are constructed by Cr₂O₃ nanoparticles uniformly encapsulated 1D porous N-doped carbon matrix. Importantly, the as-prepared Cr₂O₃/NC electrode shows a superior Li-ion battery anodic performance. Under a current density of 100 mA g⁻¹, the Cr₂O₃/NC sample has a specific discharge capacity of 640 mA h g⁻¹ after 100 cycles. Moreover, after 50 cycles at a high current density of 1000 mA g⁻¹, the sample exhibits a discharge capacity of 368 mA h g⁻¹. The outstanding Li-storage performance of the composite should be attributed to the stable porous hierarchical structure, large specific surface area and highly conductive N-doped carbon matrix.

Keywords: Hierarchical structure, Cr₂O₃/N-doped carbon composite, Bio-template method, Li-ion battery

1. INTRODUCTION

Chromium (III) oxide (Cr₂O₃) has caused widespread concern as a promising anode material for Li-ion batteries (LIBs). Compared with other transition metal oxides (TMOs) anodes, Cr₂O₃ has the advantages of high theoretical specific capacity (1058 mA h g⁻¹) and a relatively low lithium intercalation potential [1-4]. However, when Cr₂O₃ is used as anode material for LIBs, there are also disadvantages such as unsatisfied cycling stability resulted from volume change during charge/discharge process and poor rate performance caused by low conductivity [5-7].

The design and synthesis of hierarchically porous TMOs constructed by nano-sized building units have been received tremendous interest in the realization of high-performance LIBs [8-10]. In such a structure, the nano-sized primary building blocks can shorten the transmission path of Li-ions and electrons, which leads to an improvement in rate performance and the stable micro-scale secondary structures would effectively prevent self-aggregation of the primary building blocks and accommodate the volume expansion during cycling process, thereby leading to enhanced the cycle performance. Furthermore, it is reported that synthesis of Cr_2O_3 composites with a highly conductive carbonaceous material can preserve the inner active substance and enhance their conductivity and cycle life [11-15]. For example, Fu and co-authors reported that a sheet-like $\text{Cr}_2\text{O}_3/\text{C}$ composite delivered a high discharge specific capacity of $465.5 \text{ mA h g}^{-1}$ after 150 cycles under a current density of 100 mA g^{-1} [14]. Wang et al. reported that sandwich-like Cr_2O_3 -graphite intercalation composites exhibited a discharge specific of 480 mA h g^{-1} after 1000 cycles at a rate of 100 mA g^{-1} [15]. In addition, a large number of studies have shown that doping N atoms can improve the electronic conductivity of carbon-based materials and thus improve their electrochemical performance [16-18]. Therefore, a combination of porous hierarchical structure and composited with conductive N-doped carbon might lead to significant improvement of electrochemical properties for lithium-ion batteries.

Recently, the bio-template technology has become a practical approach for preparing advanced anode materials with controllable nanostructure [19-21]. In particular, such technology is simple, inexpensive and environmentally friendly. Eggshell membrane (ESM) is a kind of very useful biological template because of its unique interwoven fiber structure, large specific surface area and large quantities of the N element [22,23]. At present, many kinds of metal oxides materials with higher functionality have been synthesized by ESM template method [24-26]. However, based on literature research, there are almost no reports on using the ESM as template and carbon source to synthesize the $\text{Cr}_2\text{O}_3/\text{NC}$ composite as anode materials.

Herein, we fabricated a hierarchically porous $\text{Cr}_2\text{O}_3/\text{NC}$ composite by using ESM as bio-template and carbon source. As expected, such porous hierarchical structure with uniform encapsulated in N-doped carbon matrix can enlarge the contact area of the active materials, improve the conductivity of the electrode and electrolyte, and provides sufficient space to allow an expansion during cycling process. At a current density of 100 mA g^{-1} , the as-prepared $\text{Cr}_2\text{O}_3/\text{NC}$ composite shows an outstanding electrochemical performance with a reversible capacity of composites is 640 mA h g^{-1} after 100 cycles.

2. MATERIALS AND METHODS

2.1 Materials synthesis

Eggshell membranes (ESM) were manually removed from the eggshell of commercial hen's eggs and then washed with deionized water thoroughly. Subsequently, the ESM was soaked in a concentration of $0.020 \text{ mol/L Cr}(\text{NO}_3)_3 \cdot 9\text{H}_2\text{O}$ ethanol solution for 48h. After taking out from this solution and drying at room temperature, a pale green precursor was obtained. The final black product was acquired by calcining the pale green precursor in an N_2 atmosphere at 500°C for 2 hours.

2.2 Structure characterization

The XRD patterns of the sample were recorded on a Rigaku X-ray diffractometer (D/Max-3B) using a Cu K α radiation source. TG analysis was carried out on a Perkin Elmer thermogravimetric analyzer (TG/DTA 6300) in air atmosphere. The FE-SEM (Field emission scanning electron microscopy) images and the TEM (Transmission electron microscopy) images of as-obtained products were characterized by using Hitachi S-4800 scanning electron microscope and JEOLJEM-2100 F microscope, respectively. The specific surface area and pore size distribution were estimated from N₂ adsorption-desorption analysis which was measured on a Gas Sorption System (Micro-metrics Instruments, ASAP 2420). The XPS (X-ray photoelectron spectroscope) analysis was performed on a Kratos photoelectron spectrometer (ULTRA AXIS DLD) with monochrome Al K α (h ν = 1486.6 eV) radiation. All binding energies were calibrated by referencing to C1s (284.6 eV).

2.3 Electrochemical measurements

CR2025 coin-type cell which was applied to electrochemical measurements was composed of a working electrode, a lithium foil as counter electrode, an electrolyte, a separator, and the battery case. To fabricate the working electrode, Cr₂O₃/NC active material was adequately mixed with polyvinylidene fluoride (PVDF) as adhesive at a mass ratio of 90:10 in N-methylpyrrolidone (NMP) solvent to form a homogeneous mixture. The obtained mixture was pressed on Cu foil and punched into a disc. And then dried at 120 °C for 12 h under a vacuum. The as-obtained model test cells were assembled in an argon-filled glove box and galvanostatic charge/discharge tests were performed on a Land CT2001A automatic battery tester under the range of 0.01-3.0 V at ambient temperature. The measurements of cycling voltammetry (CV) and electrochemical impedance spectroscopy (EIS) were operated on a CHI 660C electrochemical workstation (Chenhua, Shanghai).

3. RESULTS AND DISCUSSION

Figure 1(a) displays an XRD pattern of the Cr₂O₃/NC sample after calcined 500 °C in N₂. All diffraction peaks are consistent with the standard spectrum of the hexagonal Cr₂O₃ (JCPDS no. 38-1479) [4]. No carbon peaks are found, suggesting that the carbon in this sample is amorphous. The broadened diffraction peaks demonstrate that Cr₂O₃/NC is assembled from smaller building units. The carbon content in Cr₂O₃/NC sample was determined by the thermogravimetric analysis under the air atmosphere. As shown in Figure 1(b), after heated to 800 °C, a weight loss of 3.3% was observed for pristine Cr₂O₃, which was attributed to the loss of moisture and the decomposition of the organic matters reserved on the Cr₂O₃ surface. In contrast, the residual mass of Cr₂O₃/NC composite is 65.6% after heated to 800 °C, indicating that the carbon content in the Cr₂O₃/NC composite was 31.1%.

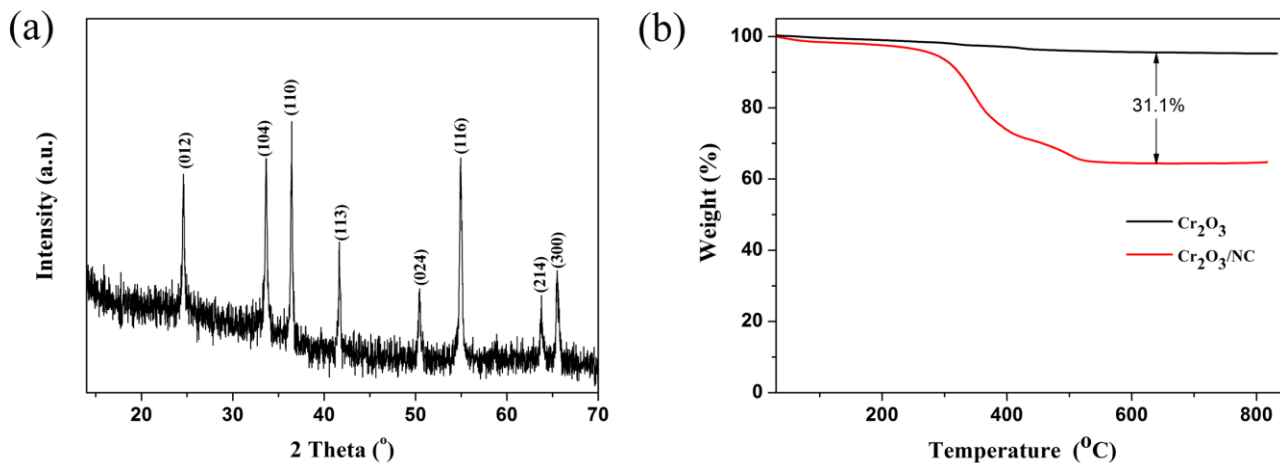


Figure 1. (a) XRD patterns of $\text{Cr}_2\text{O}_3/\text{NC}$ sample after calcined $500\text{ }^\circ\text{C}$ in N_2 ; (b) TGA curves of pristine Cr_2O_3 and $\text{Cr}_2\text{O}_3/\text{NC}$ sample.

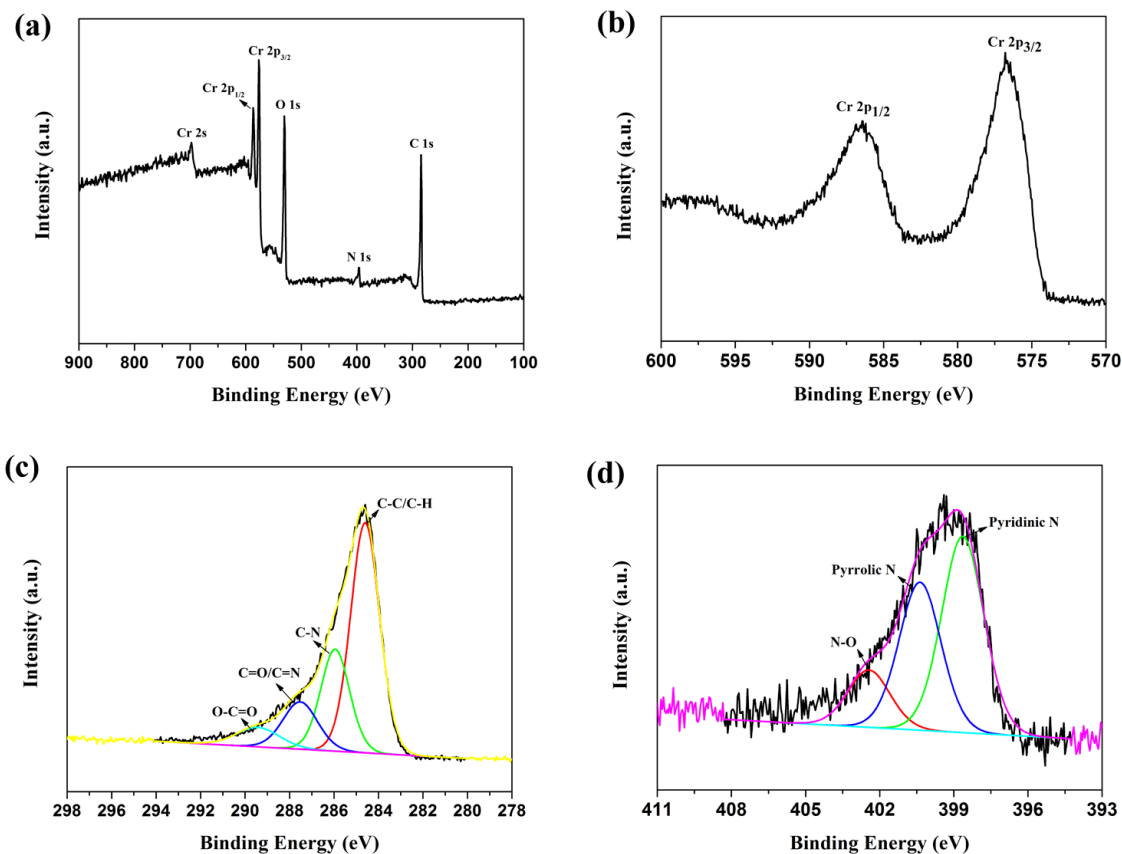


Figure 2. The XPS spectra of $\text{Cr}_2\text{O}_3/\text{NC}$ sample: (a) the wide spectrum, (b-d) high-resolution spectra for Cr 2p, C 1s and N 1s.

The compositions and elemental valence on the surface of the synthesized $\text{Cr}_2\text{O}_3/\text{NC}$ sample were characterized by XPS. The wide spectrum of the $\text{Cr}_2\text{O}_3/\text{NC}$ sample is shown in Figure 2(a). All recorded peaks in the wide spectrum are assigned to the four elements of Cr, O, N and C, indicating that the $\text{Cr}_2\text{O}_3/\text{NC}$ sample is composed of these four elements. The valence state of Cr in the $\text{Cr}_2\text{O}_3/\text{NC}$ sample is characterized by high-resolution XPS spectrum for Cr 2p. As shown in Figure 2(b), two

peaks located at 586.8 eV and 577.2 eV can be attributed to the binding energy of Cr 2p_{1/2} and Cr 2p_{3/2} in Cr₂O₃. The high-resolution XPS spectrum of carbon (Figure 2(c)) can be decomposed into four binding peaks corresponding to different carbon-containing functional groups[16]: (a) C-C/C-H group at 284.6 eV, (b) carbon in C-N at 286.1 eV, (c) C=O/C=N group at 287.7 eV), and (d) carboxylate carbon (O-C=O, 288.9 eV). In the high-resolution N 1s spectrum (Figure 2(d)), there are three peaks at around 398.5, 399.8 and 402.2 eV, which belong to pyridinic nitrogen, pyrrolic and N-O functional group, respectively [17], which originates from nitrogen-containing biomolecules present in the ESM, such as proteins, amino acids, and nucleic acids. The doping of N-atom in carbon fibers can greatly increase the electronic conductivity, which is benefit to improve the electrochemical performance.

Figure 3(a) displays the N₂ adsorption-desorption isotherms of Cr₂O₃/NC sample. It can be seen that the Cr₂O₃/NC sample presents a type IV isotherm with H3-type hysteresis loops. The pore size distribution curve (Figure 3(b)) exhibits that the Cr₂O₃/NC sample has not only mesopores derived from the accumulation of piny nanoparticles, but also macropores coming from the stacking of interweaving microfiber. The BET specific surface area of the Cr₂O₃/NC composite is 80.46 m² g⁻¹. The large BET specific surface area can not only enable active material sufficient contact with electrolyte, but also provide more reaction sites at the surface.

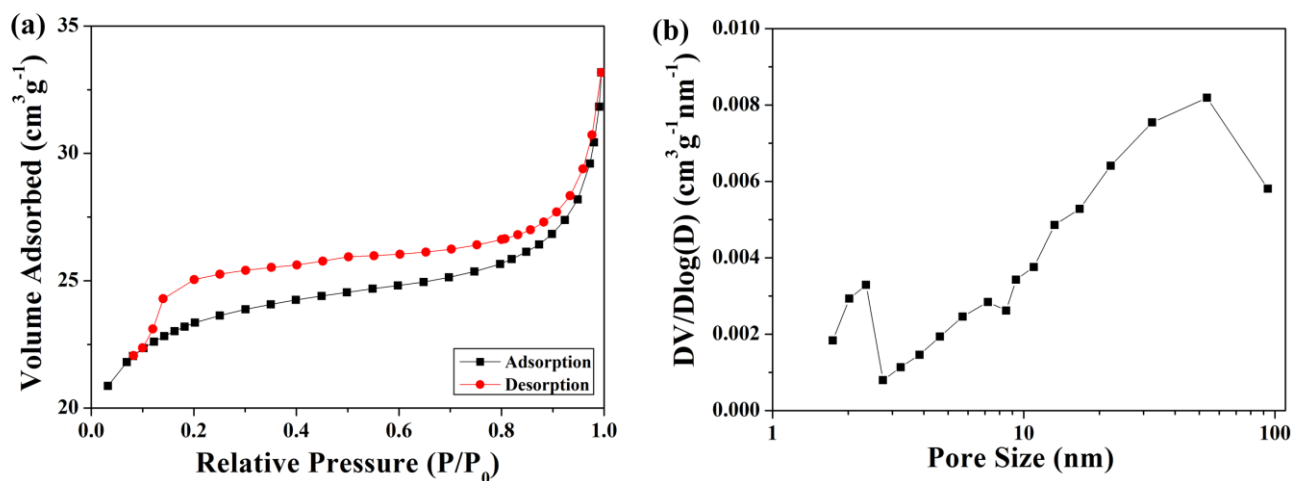


Figure 3. (a) N₂ adsorption-desorption isotherms of Cr₂O₃/NC sample; (b) the corresponding pore size distribution of Cr₂O₃/NC sample.

Figure 4(a) and (b) show the SEM image of ESM after calcined under 500 °C in N₂ atmosphere. The membrane has a porous hierarchical structure, which is composed of interwoven and conglomerate microfibers ranging from 2 to 5 μm in diameter, and the pores about 2-3 μm in size are present evidently. An overview image of the Cr₂O₃/NC sample reveals that the sample still maintains porous hierarchical structure of the ESM template (Figure 4(c)). The fibers with a considerable shrinkage are about 0.3-1.0 μm in diameter. From higher magnification SEM images (Figure 4(d)), it is seen that the interwoven fiber of the Cr₂O₃/NC composite is composed of piny nanoparticles, which is different from the smooth carbon fiber of ESM.

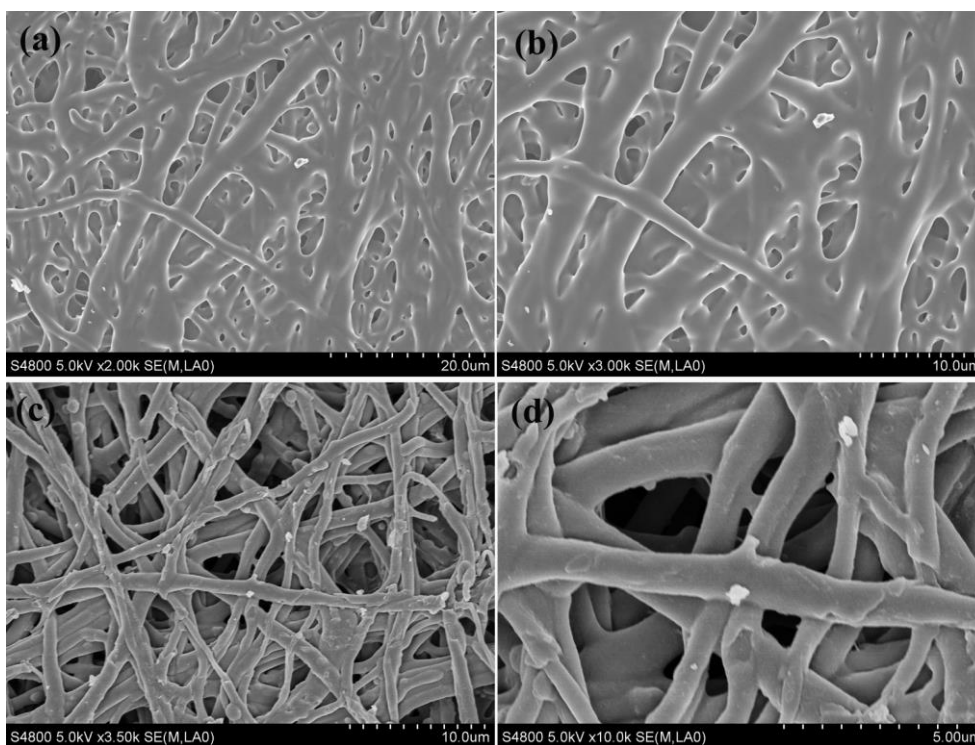


Figure 4. (a, b) SEM images of ESM after calcined at 500 °C in N₂; (c, d) SEM images of Cr₂O₃/NC sample after calcined at 500 °C in N₂.

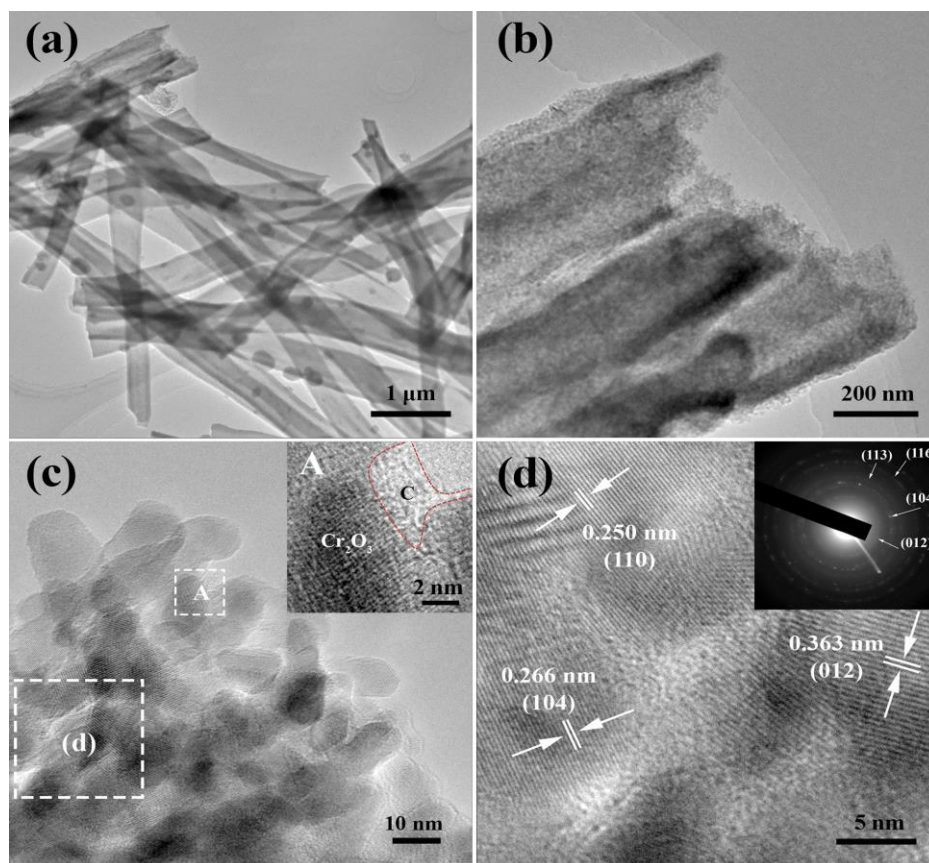


Figure 5. TEM images of Cr₂O₃/NC sample; (a) Low-magnification; (b, c) high-magnification; (d) HRTEM and SEAD pattern(inset).

The morphology and microstructure of $\text{Cr}_2\text{O}_3/\text{NC}$ sample can be further confirmed by the TEM characterizations (Figure 5). The overall morphology of the as-synthesized $\text{Cr}_2\text{O}_3/\text{NC}$ sample is highlighted in Figure 5(a), which consists of interwoven microfibers with a diameter of 300-1000 nm. Figure 5(b) shows a single fiber, which is a porous structure with a diameter of about 800 nm. By closer observation (Figure 5(c) insert), It can be found that there is a 2-3 nm thick carbon layer around the Cr_2O_3 nanoparticles, indicating that the porous microfibers are constructed by the Cr_2O_3 nanoparticles uniformly encapsulated in the N-doped carbon matrix. The mean size of Cr_2O_3 nanoparticles is in the range of 5-20 nm. As shown in the Figure 5(d), The lattice fringes are clearly observed with the spacing of 0.250, 0.266 and 0.363 nm, which is in good agreement with the spacing of the (110), (104) and (012) plane of the Cr_2O_3 , respectively. The selected-area electron diffraction (SAED) pattern reveals a polycrystalline nature of $\text{Cr}_2\text{O}_3/\text{NC}$ sample (inset of Figure 5(d)).

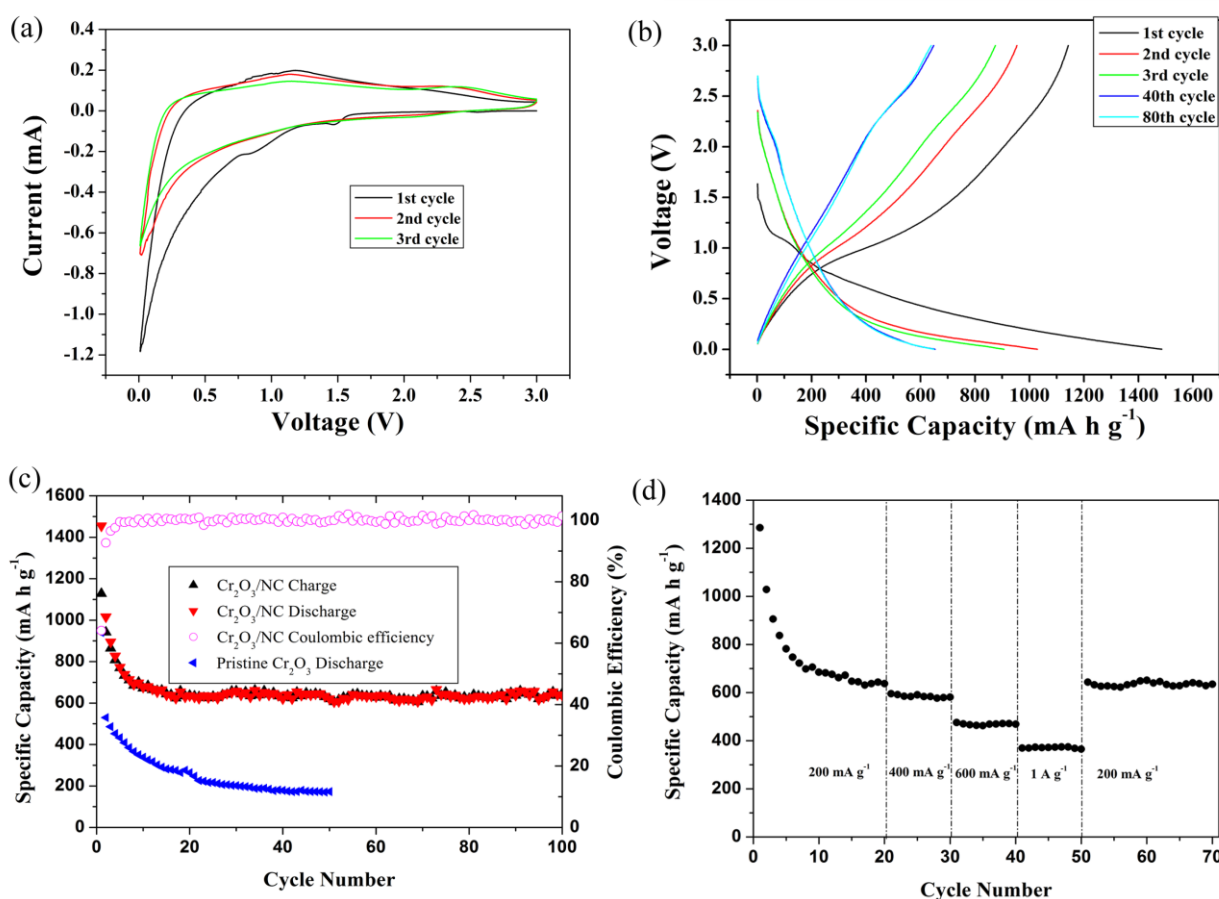


Figure 6. (a) CV curves $\text{Cr}_2\text{O}_3/\text{NC}$ electrode at a scan rate of 0.5 mV s^{-1} ; (b) Charge-discharge profiles of $\text{Cr}_2\text{O}_3/\text{NC}$ electrode at 100 mA g^{-1} ; (c) Cycling performance of $\text{Cr}_2\text{O}_3/\text{NC}$ electrode and pristine Cr_2O_3 electrode at 100 mA g^{-1} ; (d) Rate performances of $\text{Cr}_2\text{O}_3/\text{NC}$ electrode at different current densities.

The first three consecutive cyclic voltammetry (CV) curves of $\text{Cr}_2\text{O}_3/\text{NC}$ electrode are shown in Figure 6(a). There is a substantial difference in the CV curves between the first and the following cycles. In the first cycle, it can be observed that an irreversible cathode peak appearing at around 0.80 V is result of the decomposition of the electrolyte and the formation of the solid electrolyte interface

(SEI) film. The significant cathode peak appears at 0.01 V, corresponding to the reduction of Cr_2O_3 to Cr^0 . The anodic peak appearing in the range of 0.6-1.6 V corresponds to the oxidation of Cr^0 to Cr_2O_3 [14]. The position and the intensity of the cathode and anode peaks were almost unchanged after the first cycle, indicating that the electrode has excellent cycle stability during charge and discharge. Figure 6(b) displays the representative charge-discharge profiles of the $\text{Cr}_2\text{O}_3/\text{NC}$ electrode. It is observed that the $\text{Cr}_2\text{O}_3/\text{NC}$ electrode exhibits the initial charge and discharge capacities of 1141 and 1480 mA h g^{-1} , respectively, and the initial Coulombic efficiency is 77%. In addition, the charge-discharge curves of the 40th and 80th cycle are almost coincident, indicating that the material has superior cycle performance.

The cyclic performances of pristine Cr_2O_3 electrode and $\text{Cr}_2\text{O}_3/\text{NC}$ electrode were investigated (Figure 6(c)). The Coulombic efficiency of $\text{Cr}_2\text{O}_3/\text{NC}$ electrode is 89.6% in the 2nd cycle and remains steadily higher than 98% after the 5 cycles. The discharge specific capacity of $\text{Cr}_2\text{O}_3/\text{NC}$ electrode can retain 640 mA h g^{-1} after 100 cycles. As a comparison, the pristine Cr_2O_3 electrode exhibits a discharge specific capacity of 172 mA h g^{-1} after 50 cycles at the same current density. Even cycled at higher current, the $\text{Cr}_2\text{O}_3/\text{NC}$ still exhibits an excellent Li-storage performance shown in Figure 6(d). It can deliver the discharge specific capacity of 630, 581, 468, and 368 mA h g^{-1} under the current density of 200, 400, 600 and 1000 mA g^{-1} , respectively. Moreover, when the current density is restored to 200 mA g^{-1} , the discharge specific capacity also recovers to 628 mA h g^{-1} , indicating that the $\text{Cr}_2\text{O}_3/\text{NC}$ electrode has better stability and reversibility.

Figure 7 shows the electrochemical impedance measurement of the pristine Cr_2O_3 and $\text{Cr}_2\text{O}_3/\text{NC}$ electrodes from 100 kHz to 0.01 Hz. Both Nyquist plots display a depressed semicircle at the high and middle frequency and a straight line at the low frequency. The charge transfer resistance (R_{ct}) of the $\text{Cr}_2\text{O}_3/\text{NC}$ electrode (89 Ohm) is obviously smaller than that of pristine Cr_2O_3 one (343 Ohm), suggesting that the conductivity of the $\text{Cr}_2\text{O}_3/\text{NC}$ electrode is obviously improved.

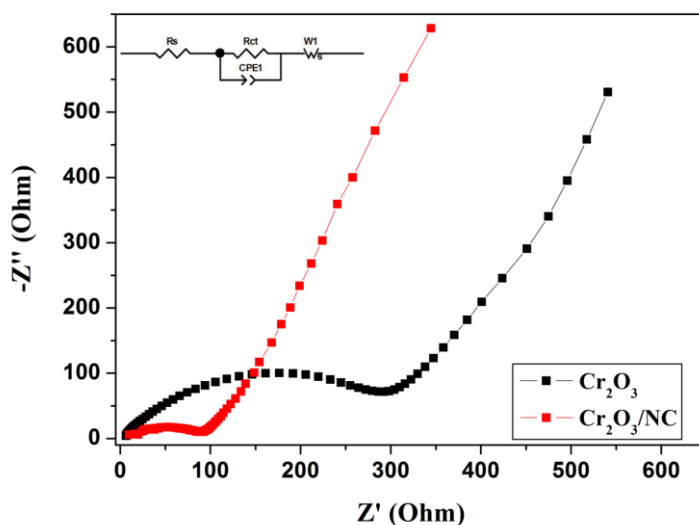


Figure 7. EIS spectra of the $\text{Cr}_2\text{O}_3/\text{NC}$ electrode and the pristine Cr_2O_3 electrode.

Table 1. Comparison of electrochemical performance of this work with previously reported Cr₂O₃-based materials.

Materials	Synthesis method	Current density/rate mA g ⁻¹	Cycle number	Specific capacity (mAh g ⁻¹)	Ref.
Cr ₂ O ₃ quantum nanodots	electrospinning	100	100	527	[2]
Mesoporous Cr ₂ O ₃ sheet	Solution combustion	100	55	480	[3]
Cr ₂ O ₃ -C nanospheres	Non-sacrificial template	200	35	600	[4]
Cr ₂ O ₃ nanostructured thin film	Pulsed laser deposited	100	50	543	[6]
Mesoporous Cr ₂ O ₃	Vacuum assisted impregnation	100	100	540	[7]
Mesoporous carbon-Cr ₂ O ₃	Template method	50	80	639	[11]
Carbon-coated grapheme-Cr ₂ O ₃ composites	Hydrothermal method	100	100	550	[12]
Cr ₂ O ₃ @C@G composites	Spray drying	100	120	648	[13]
Cr ₂ O ₃ carbon nanocomposites	Sol-gel method	100	150	465	[14]
Sandwich-like Cr ₂ O ₃ - graphite	Intercalation-transformation	100	200	420	[15]
Hierarchically porous Cr ₂ O ₃ /N-doped carbon	Bio-template method	100	100	640	This work
		1000	50	368	

Table 1 gives the comparison of the results on Cr₂O₃-based anode materials reported in the literature, including their morphologies, synthesis method and Li-ion battery anodic performance with the results of this work. Obviously, the as-synthesized Cr₂O₃/NC sample in this work shows better cycle stability and superior high rate performance. The reasons that our sample exhibits such outstanding properties may be ascribed to its stable porous hierarchical structure and highly conductive N-doped carbon matrix. On the one hand, the N-doped carbon matrix uniformly wrapped around the Cr₂O₃ nanoparticles can inhibit the agglomeration of the Cr₂O₃ nanoparticles and improve the electrical conductivity of the electrode. On the other hand, the stable porous hierarchical structure can enable sufficient contact between the electrolyte and active material and provides more reaction sites on the surface, resulting in the increase in specific capacity. Moreover, the porous structure possesses the ability to greatly facilitate Li⁺ transfer and effectively alleviate the structural strain caused by volume change during repeated charge-discharge cycles, leading to enhanced cycle performance.

4. CONCLUSIONS

The hierarchically porous Cr₂O₃/NC composite has been successfully synthesized by using bio-template method. The ESM used in this work plays a dual role, which acts as templates to adsorb metal ions and acts as carbon sources to construct a N-doped conductive carbon matrix. As a result, the Cr₂O₃/NC electrode shows high reversible specific capacity, outstanding cyclability and rate capability. The superior Li-ion battery anodic performance of the Cr₂O₃/NC composite make it promising as an anode materials for advanced LIBs.

ACKNOWLEDGEMENTS

This work was supported by the International Science & Technology Cooperation Program of China (2016YFE0115100), National Natural Science Foundation of China (21771060, 61271126 and 21305033), Program for Science and Technology Project of Heilongjiang province (B201414).

References

1. L. Dupont, S. Grugeon, S. Laruelle, J.M. Tarascon, *J. Power Sources*, 164 (2007) 839.
2. T. Yang, Z. Chen, H. Zhang, M. Zhang, T. Wang, *Electrochim. Acta*, 217 (2016) 55.
3. J.Z.Q. Cao, M.L. Qin, B.R. Jia, L. Zhang, Q. Wan, M.S. Wang, A.A. Volinsky, X.H. Qu, *Electrochim. Acta*, 139 (2014) 76.
4. L.Y. Jiang, S. Xin, X.L. Wu, H. Li, Y.G. Guo, L.J. Wan, *J. Mater. Chem.*, 20 (2010) 7565.
5. S.M. Abbas, N. Ahmad, U.A. Rana, S.U.D. Khan, S. Hussain, K.W. Nam, *Electrochim. Acta*, 212 (2016) 260.
6. S. Khamlich, Z. Nuru, A. Bello, M. Fabiane, J. Dangbegnon, N. Manyala, M. Maaza, *J. Alloy. Compd.*, 637 (2015) 219.
7. H. Liu, X. Du, X. Xing, G. Wang, S.Z. Qiao, *Chem. Commun.*, 48 (2012) 865.
8. Y. Hao, S.B. Wang, J.S. Zeng, H.L. Li, P.H. Yang, B.H. Liu, S.C. Zhang, Y.L. Xing, *Ceram. Int.*, 44 (2018) 1321.
9. W.K. Zhai, Y.M. Xu, X.L. Cheng, S. Gao, X.F. Zhang, H. Zhao, L.H. Huo, *Mater. Lett.*, 145 (2015) 287.
10. H.M. Liang, Z.X. Wang, H.J. Guo, X.H. Li, *Ceram. Int.*, 43 (2017) 11058.
11. B.K. Guo, M.F. Chi, X.G. Sun, S. Dai, *J. Power Sources*, 205 (2012) 495.
12. W. Yue, S. Tao, J. Fu, Z. Gao, Y. Ren, *Carbon*, 65 (2013) 97.
13. Y. Xiang, Z. Chen, C.Y. Chen, T.H. Wang, M. Zhang, *J. Alloy. Compd.*, 724 (2017) 406.
14. Y. Fu, H.B. Gu, X.R. Yan, J.R. Liu, Y.R. Wang, J.N. Huang, X.Y. Li, H.L. Lv, X.Z. Wang, J. Guo, G.X. Lu, S. Qiu, Z.H. Guo, *Chem. Eng. J.*, 277 (2015) 186.
15. F. Wang, W. Li, M. Hou, C. Li, Y. Wang, Y. Xia, *J. Mater. Chem.*, A 3 (2015) 1703.
16. V. Selvamani, R. Ravikumar, V. Suryanarayanan, D. Velayutham and S. Gopukumar, *Electrochim. Acta* 190 (2016) 337.
17. L.Y. Li, P.C. Liu, K.J. Zhu, J. Wang, G.A. Tai, J.S. Liu, *Electrochim. Acta*, 235 (2017) 79.
18. V. Selvamani, V. Suryanarayanan, D. Velayutham and S. Gopukumar, *New J. Chem.*, 41 (2017) 3297.
19. J.F. Wang, W. Liu, J.X. Chen, H.L. Wang, S. Liu, S.G. Chen, *Electrochim. Acta*, 188 (2016) 210.
20. L.F. Chen, S.X. Ma, S. Lu, Y. Feng, J. Zhang, S. Xin, S.H. Yu, *Nano Res.*, 10 (2017) 1.
21. D.L. Yan, Y. Zhang, X.Y. Zhang, Z.Z. Yu, Y.Y. Zhao, G.S. Zhu, G.C. Chen, C.G. Ma, H.R. Xu, A.B. Yu, *Ceram. Int.* 43 (2017) 9235.
22. D. Yang, L. Qi, J. Ma, *Adv. Mater.*, 14 (2002) 1543.

23. J.F. Li, G.T. Zan, Q.S. Wu, *J. Mater. Chem.*, A 4 (2016) 9097.
24. J.F. Li, W. Zhang, G.T. Zan, Q.S. Wu, *Dalton Trans.*, 45 (2016) 12790.
25. Q. Dong, H.L. Su, J.Q. Xu, D. Zhang, R.B. Wang, *Mater. Lett.*, 61 (2007) 2714.
26. B. Pan, M. Park, H.Y. Kim, S.J. Park, *J. Alloy. Compd.*, 699 (2017)73.

© 2018 The Authors. Published by ESG (www.electrochemsci.org). This article is an open access article distributed under the terms and conditions of the Creative Commons Attribution license (<http://creativecommons.org/licenses/by/4.0/>).